

A regression approach to the mapping of bio-physical characteristics of surface sediment using in situ and airborne hyperspectral acquisitions

Elsy Ibrahim¹  · Wonkook Kim² · Melba Crawford³ · Jaak Monbaliu⁴

Received: 31 January 2016 / Accepted: 29 November 2016 / Published online: 3 January 2017
© Springer-Verlag Berlin Heidelberg 2016

Abstract Remote sensing has been successfully utilized to distinguish and quantify sediment properties in the intertidal environment. Classification approaches of imagery are popular and powerful yet can lead to site- and case-specific results. Such specificity creates challenges for temporal studies. Thus, this paper investigates the use of regression models to quantify sediment properties instead of classifying them. Two regression approaches, namely multiple regression (MR) and support vector regression (SVR), are used in this study for the retrieval of bio-physical variables of intertidal surface sediment of the IJzermonding, a Belgian nature reserve. In the regression analysis, mud content, chlorophyll *a* concentration, organic matter content, and soil moisture are estimated using radiometric variables of two airborne sensors, namely airborne hyperspectral sensor (AHS) and airborne prism experiment (APEX) and using field hyperspectral acquisitions by analytical spectral device (ASD). The performance of the two regression

approaches is best for the estimation of moisture content. SVR attains the highest accuracy without feature reduction while MR achieves good results when feature reduction is carried out. Sediment property maps are successfully obtained using the models and hyperspectral imagery where SVR used with all bands achieves the best performance. The study also involves the extraction of weights identifying the contribution of each band of the images in the quantification of each sediment property when MR and principal component analysis are used.

Keywords Intertidal sediment · Hyperspectral · Multiple regression · Support vector regression · AHS · APEX · Mud · Chlorophyll *a* · Organic matter · Moisture

1 Introduction

A balance of an intertidal flat results due to the net effect of biological, physical, and sedimentological factors and processes (Fig. 1). Non-cohesive sandy sediments behave autonomously depending on their diameter and density, while cohesive silt and clay particles aggregate and act in groups (Mitchener and Torfs 1996; Amos et al. 1997). Furthermore, microorganisms stabilize the sediment surface by secreting mucilaginous films or mucus (Lundkvist et al. 2007; Murphy et al. 2009), while other organisms may destroy the “biostabilizing” structure of the sediment and thus weaken it (Herman et al. 2001; Widdows and Brinsley 2002). The importance of such sediment characteristics in determining sediment stability leads to a need for frequent field data collection, especially due to the high temporal variability of intertidal areas (Hakvoort et al. 1997). Thus, traditional field sampling is often inefficient on intertidal flats. Remote sensing offers an alternative to traditional

This article is part of the Topical Collection on the *13th International Conference on Cohesive Sediment Transport in Leuven, Belgium 7–11 September 2015*

Responsible Editor: Michael Fettweis

✉ Elsy Ibrahim
eibrahim@ndu.edu.lb

¹ Notre Dame University-Louaize, Zouk Mosbeh, Lebanon

² Korean Institute of Ocean Science and Technology, Gyeonggi-do, South Korea

³ Purdue University, Indiana, USA

⁴ Katholieke Universiteit Leuven, Leuven, Belgium

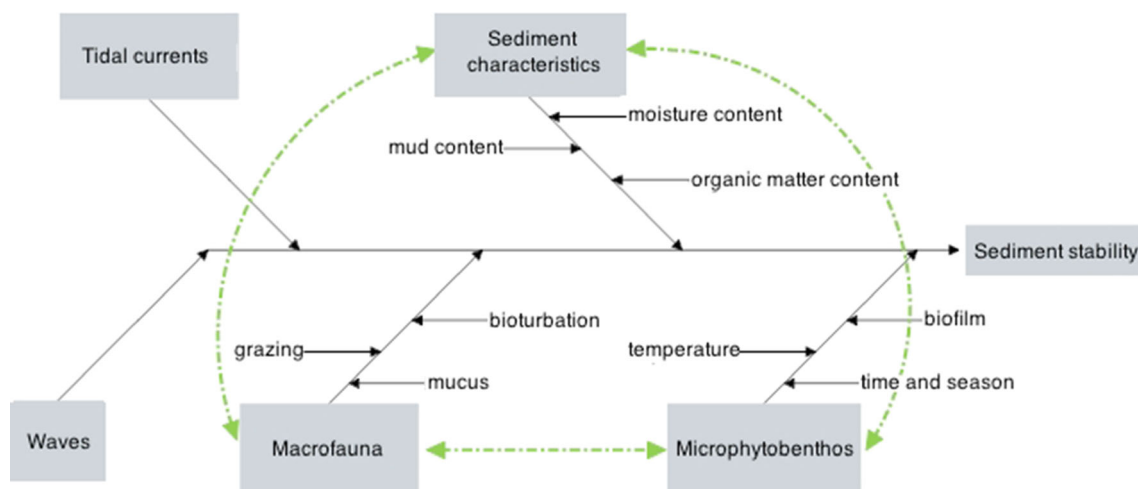


Fig. 1 Major aspects influencing sediment stability of an intertidal flat

field acquisitions and has been gaining popularity in environmental applications that include sediment-related studies (Rainey et al. 2003; Diafas et al. 2013).

Classification of imagery, supervised and unsupervised, is a basic and centrally utilized image processing tool for sediment characterization. Depending on the nature of the study area and the type of required classes, supervised classification can vary in difficulty. Spectral unmixing techniques have also been used to distinguish sediment classes by selecting spectral end-members where areas are heterogeneous (Yates et al. 1993; Rainey et al. 2003). In any case, classes of sediment types need to be defined for these approaches. Defining lake and forest classes for landuse, for example, is relatively simpler than defining the boundary between classes of moisture content of sediments due to moisture's gradual variation. Generally, sediment classes have been determined using case-specific field data or from experience and intuition, whereby the class boundaries for a sediment property were often defined using an ad-hoc procedure (Defew et al. 2002). Tables 1 and 2 (intermediate) show examples of several thresholds used by researchers to specify classes of four vital sediment properties, namely moisture content (MC), chl *a* content, organic matter content (OM), and mud content (MUC), where "mud" refers to cohesive particles smaller than 63 μm . A number of the references in these tables based their choice of classes on their experience and knowledge of the study areas (Yates et al. 1993; Thomson et al. 2003; Smith et al. 2004) or visual assessment (Barille et al. 2011). Other studies defined the classes according to erosion shear stress (Hakvoort et al. 1998) or such that they were physically meaningful and led to a similar distribution of field samples for each class (Deronde et al. 2006; Adam et al. 2006). On the other hand, the grain-size classes obtained in one of the studies were defined using ternary plots (Flemming 2000).

Furthermore, others classified various imagery using a uniform set of classes that were based on a combined view of all the available field data of the same site from various years (Ibrahim and Monbaliu 2009). Finally, one of the studies used classes achieved from unsupervised classification and the correspondence of field data to the resulting clusters (Ibrahim and Monbaliu 2013).

Although these case-dependent classes lead to useful classification results, classification accuracy is highly dependent on the choice of classes (Ibrahim and Monbaliu 2013). This case dependency makes comparison of results between sites and even images of the same site very challenging, creating a major obstacle in temporal studies. Thus, as an alternative to the use of such defined classes, regression modeling can be used for finding relationships between field sampled values and surface reflectance acquired by field, airborne, or spaceborne sensors (Ibrahim et al. 2014).

The objective of this paper is to assess the use of regression models to quantify sediment properties for an intertidal flat in Belgium using field and airborne hyperspectral data. Such regression approaches have been mostly used for grain-size mapping of surface sediment, e.g., Yates et al. (1993), Rainey et al. (2003), and Van der Wal and Herman (2007). Yet, this work attempts to address the quantification and mapping of sediment mud content, chlorophyll *a* content, organic matter content, and soil moisture using multiple regression (MR) and support vector regression (SVR).

2 Study area

The IJzermunding is located at the outlet of the IJzer river at the Belgian coast and consists of dunes, marshes and mudflats (Fig. 2). It is a small nature reserve of about 130 ha that since 1994 has been classified as an EC Special Protection

Table 1 Examples of thresholds used to describe grain-size distribution and moisture content where “mud” refers to cohesive particles smaller than 63 μm

Reference	Grain size	MC		
Yates et al. (1993)	Muddy	>20% mud		
Hakvoort et al. (1998)	Sandy mud	<25% mud		
	Muddy sand	>25 & <50		
	Mud	>50&<85		
	Clayey mud	>85		
	Flemming (2000)	Sand	<5% mud	
Flemming (2000)	Slightly muddy sand	>5 & <25		
	Muddy sand	>25 & <50		
	Sandy mud	>50 & <75		
	Slightly sandy mud	>75 & <95		
	mud	>95		
Thomson et al. (2003)	Sand	<30% mud		
	Muddy sand	>30 & <50		
	Mud	>50		
Smith et al. (2004)	Low	<50 μm mean gs	Low	<20%
	Medium	>50 & <100	Medium	>20 & <30
	High	>100	High	>30
Deronde et al. (2006)	Sand	<30% mud	Low	<30%
	Mud	>30	High	>30
Adam et al. (2006)	Sand	<15% mud	Dry	<20%
	Loamy sand	>15 & <30	Wet	>20 & <30
	Clayey loam	>30	Very wet	>30 & <40
	Sat	>40		
Ibrahim and Monbaliu (2009)	Low	<10% mud	Low	<20%
	Interm	>10 & <40	Interm	>20 & <40%
	High	>40%	High	>40%
Barille et al. (2011)	Fine Sand	88.8% > 125 μm & <250 μm		
	Mud	>97% mud		
Ibrahim and Monbaliu (2013)	Low	<10% mud	Low	<20%
	High	>10% mud	High	>20% mud

Table 2 Examples of thresholds used to describe Chl *a* content and organic matter content

Reference	Chl <i>a</i>	OM		
Smith et al. (2004)	Low	<50 mg/m ²	Low	<2%
	Medium	>50 & <100	Medium	>2% & <5%
	High	>50	High	>5
Deronde et al. (2006)	Low	<40 mg/m ²	Low	<2%
	High	>40	Interm	>2% & <4%
Adam et al. (2006)	Low	20 mg/m ²	Low	<2%
	Interm	>20 & <40	Interm	>2% & <4%
	High	>40	High	>4%
Ibrahim and Monbaliu (2009)	Low	40 mg/m ²	Low	<4%
	Interm	>40 & <80	Interm	>4 & <10
	High	>80	High	>10
Ibrahim and Monbaliu (2013)	Low	<80% mud	Low	<3%
	High	>80%	High	>3%

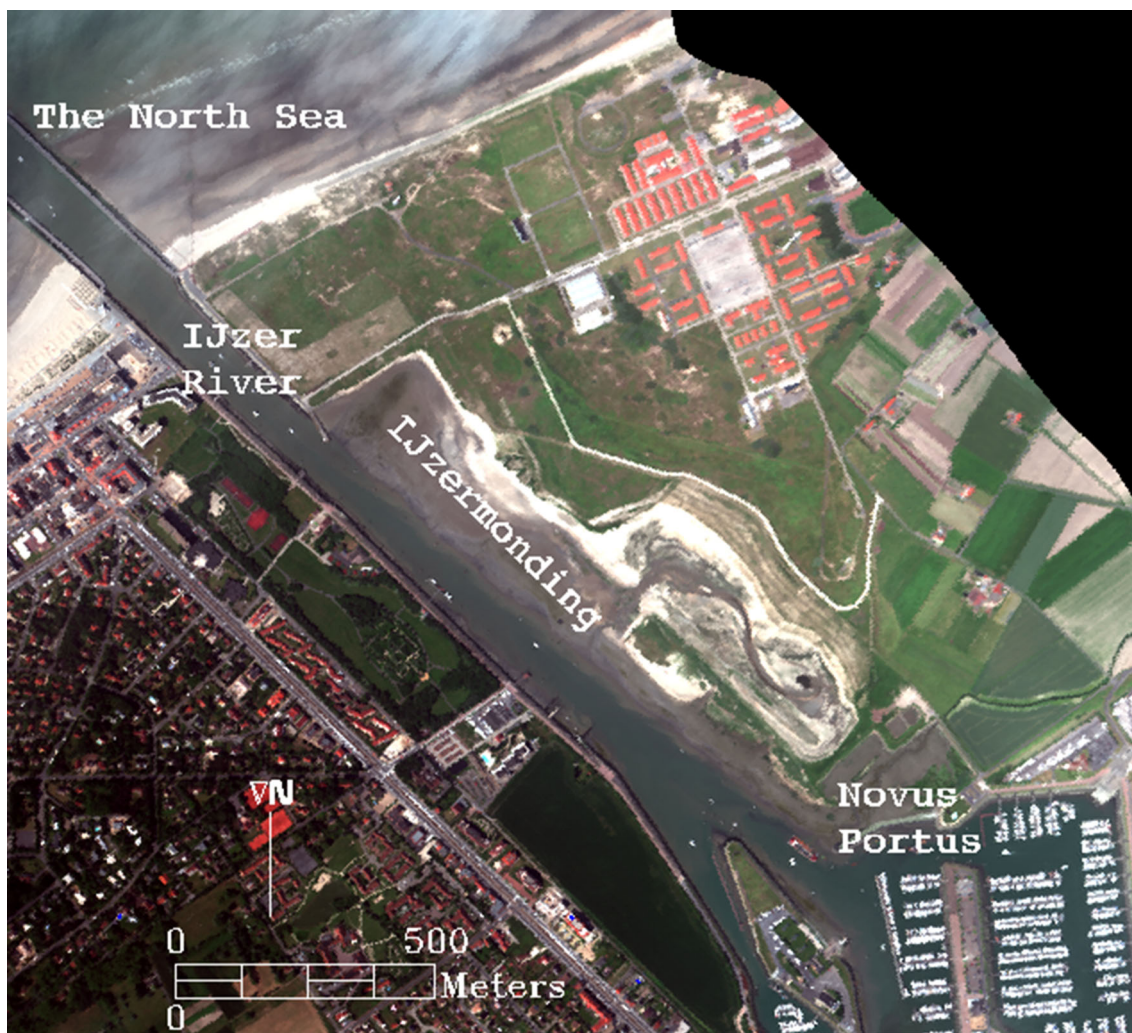


Fig. 2 The location of the IJzermonding nature reserve

Area for birds. In 1999, a nature restoration project was initiated that aimed at restoring natural gradients taking into consideration their important function of coastal defence (Hoffman et al. 2005). Accordingly, buildings, roads, docks, and a former naval base were removed resulting in larger areas of mudflats and marshes (Herrier and Nieuwenhuys 2005). Tides are semidiurnal with a mean tidal range of 3.2 m at neap and 5 m at spring tide. The average tide has a mean flood duration of 5h34' and mean ebb duration of 6h51' (Giardino et al. 2009).

3 Flight campaigns

Two hyperspectral images of the IJzermonding were considered for this study and were acquired at cloud-free and low-tidal conditions:

- On the 17th of June 2005, an image was acquired by the airborne hyperspectral sensor (AHS) resulting in

a 3.4 m × 3.4 m pixel-sized image. Raw data was radiometrically calibrated for system errors and geometrically corrected using the PARGE software (ReSe Applications Schlapfer, Switzerland). For the atmospheric correction, sunphotometer measurements were acquired simultaneously to the overflight to estimate the amount of water vapor and the aerosol concentration. Then, the atmospheric correction was carried out using ATCOR4 which is based on the radiometric transfer model MODTRAN 4 (Richter and Schläpfer 2002). The radiometric, atmospheric, and geometric corrections were done by VITO (Vlaamse Instelling voor Technologisch Onderzoek; Flemish Institute for Technological Research)

- On the 9th of July 2013, an image was acquired by the airborne prism experiment (APEX) resulting in a 2.317 m × 2.317 m pixel-sized image. The geometric correction was performed using a C++ module developed by VITO and is based on direct georeferencing.

Input data from the sensor’s GPS/IMU, boresight correction data, and the Flanders DEM were further used during the geometric correction process. The atmospheric correction was carried out with the MODTRAN4 radiative transfer code (Richter and Schläpfer 2002). The radiometric, spectral, and geometric calibrations were performed using calibration cubes generated from data measured and collected on the APEX calibration home base (CHB) hosted at DLR Oberpfaffenhofen, Germany (Gege et al. 2009).

The good quality bands of the two images are described in Tables 3 and 4. For each of the modules: visible (VIS), near-infrared (NIR), and short wave-infrared (SWIR), the number of bands, the spectral range, and the full width at half maximum (FWHM) are listed.

4 Field campaigns

Field campaigns were carried out at low tide to accompany the acquired images. For each campaign, sampling sites were chosen based on field knowledge to include the highest diversity in sediment properties. The coordinates of the sampled sites were determined by a differential global positioning system, and surface reflectance was measured by an analytical spectral device (ASD) spectrometer. ASD records the reflectance from 350 to 2500 nm. Its spectral resolution is 3 nm for the region 350–1000 and 10 nm for the 1000–2500 nm region. These spectral measurements were performed at a height of 0.7 m with a nadir looking 25° field of view.

The samples were collected of the upper 2 mm of the sediment to be tested for chl *a* content, moisture content, organic matter content, and mud content with a 2.5 cm diameter contact corer that freezes a 2 mm layer. Pigments were extracted using 90% acetone, identified using the High-performance liquid chromatography (HPLC) method (Wright et al. 1991) and quantified using a calibration with commercial standards. The moisture content of a sample was determined by calculating the weight difference after a 12-h drying process at 105 °C. Grain size was determined in a Coulter Counter for the 2005 campaigns and a Malvern Instrument Mastersizer2000 for the 2013 campaign. Finally, organic matter content was determined by calculating the

Table 3 The relevant 19 bands of the AHS image of the IJzermondig acquired in 2005

Module	Spectral range (nm)	Band	FWHM (nm)
VIS	445–689	1–8	27–30
NIR	718–1004	9–18	27–30
SWIR	1419–1824	19	159

Table 4 The relevant 99 bands of the APEX image of the IJzermondig acquired in 2013

Module	Spectral range (nm)	Band(s)	FWHM (nm)
VIS	414–698	1–57	3.4–13.8
NIR	702–1350	58–149	4.8–16.7
SWIR	1974–2337	220–271	8.2–12.0

difference in weight between the sample before and after burning at 600 °C for 2 h.

In 2005, 28 sites were sampled four days before the flight. To account for the variability within one pixel, two or three replicate samples (within 2 m) were taken leading to 80 samples. Then, 36 spectral measurements were acquired where for a number of sites, 2 or 3 replicates were considered. In 2013, the field campaign was carried out the day after the overflight. Field sampling at 29 sites was considered with one sample per site in addition to 43 spectral measurements as they included replicates. Table 5 shows an overview of the analyzed parameters per campaign.

5 Methodology

5.1 Feature extraction

Dimensionality can be a critical factor when working with remote sensing data, whereby a successful reduction of the number of dimensions can lead to an increase in computational efficiency and estimation accuracy. There are several powerful feature extraction techniques (Kumar et al. 2001; Jolliffe 1986), where principal component analysis (PCA) is one of the most popular. PCA provides a condensed description of multivariate data and is a linear transformation method where a new coordinate system for the data set is chosen such that the greatest variance by a projection of

Table 5 Overview of the field data acquired in 2005 and 2013

	Min	Average	Max
2005			
chl <i>a</i> (mg/m ²)	0	71	201
MC (%)	6	36	71
MUC (%)	0	36	94
OM (%)	2	7	21
2013			
chl <i>a</i> (mg/m ²)	7	34	97
MC (%)	1	36	78
MUC (%)	6	40	90
OM (%)	0.5	5	15

the data comes to lie on the first axis (first principal component), the second greatest variance on the second axis, etc. Lillesand and Kiefer (2015). This PCA approach was tested in this paper to assess its impact on the regression models and was compared to the use of all spectral bands.

5.2 Regression models and their performance

Multiple regression (MR) (Draper and Smith 1998) was utilized along with support vector regression (SVR) (Drucker et al. 1996). Multiple regression is a more extended approach to regression than simple linear regression, where it is utilized to predict the value of a variable based on the value of several variables. On the other hand, SVM considers a kernel function to transform a nonlinear learning problem into a linear learning problem. A structural risk minimization (SRM) principle was used to identify the most suitable linear approximation function as it controls the empirical errors.

Field samples with corresponding ASD data and with corresponding airborne spectra were used to test the regression and feature reduction approaches. To derive the generalized estimation performance of the regression for each sediment property, the accuracy of regression estimates was evaluated using mutually independent training and validation data sets. Thus, an *m*-fold cross-validation scheme was used. In the validation scheme, the total samples were first randomly divided into training and validation sets with the relative portions of 75 and 25%, respectively. For this study, *m* = 4, thus the 75% (training)/25% (testing) division was repeated four times. The regressor was thus trained and applied to the validation samples to produce the accuracy estimates. Thus, for each sediment property, four runs were done for each of MR and SVR. Furthermore, for each property and regression approach, the results using all bands were compared to the use of PCs.

For the performance measure, absolute mean percent difference (APD) as defined below and the correlation sum-of-squared-difference (Corr) were used. The use of the two measures is important since APD is a measure for estimation of uncertainty while Corr shows the overall performance of the estimation.

$$APD = 100 * \sum_{i=1}^n |(v^{estimated} - v^{insitu})/v^{insitu}| \quad (1)$$

where $v^{estimated}$ and v^{insitu} denote the estimated variable values and the in-situ measured values, respectively. APD represents the variance of estimation results, e.g., an APD = 30% means the regression estimates have an average of 30% uncertainty in both directions. Thus, high performance of a regression refers to low uncertainty and high correlation.

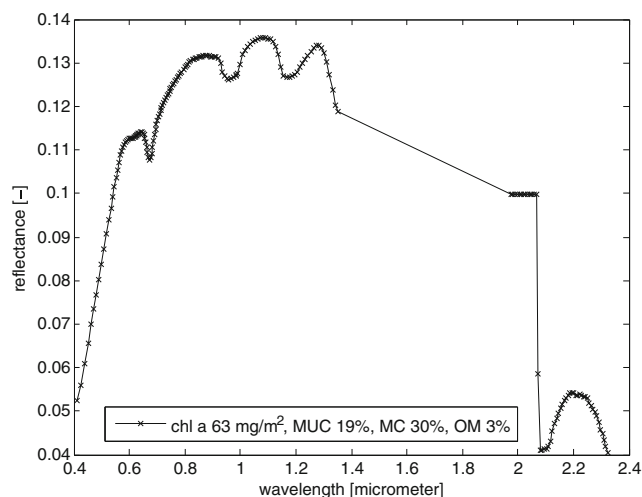


Fig. 3 2013 field spectrum resampled to APEX bands

5.3 Identifying important spectral features

Due to the nature of SVR, it is not simple to obtain the bands that were critical in quantifying certain properties. Yet, with MR, it is possible to retrieve those bands. With PCA and the regression analysis, a weight vector, *W*, is obtained from the original data *X*, e.g., an image, that is a set of *N* pixels and *n* features (bands).

$$V = WX \quad (2)$$

where *X* is the *N* × *n* original data, *V* is the of *N* × *P* transformed data where *P* corresponds to the number of selected PCs, and *W* is the *n* × *P* weight vector. Multiple regression is

$$Z = KV \quad (3)$$

where *K* is the *P* × *P* weight matrix and *Z* is *N* × *P* final data matrix.

Thus, the coefficient *KW* can be retrieved.

$$Z = KWX \quad (4)$$

6 Results

6.1 Feature reduction

When using ASD spectra to quantify sediment properties of imagery, these spectra were resampled to the bands of the

Table 6 The contribution of five PCs to the total variance in the data

2005 ASD	2005 AHS	2013 ASD	2013 APEX
98.7%	99.7%	99.1%	99.4%

Table 7 2005 ASD Summary of regression results using all bands

Property	MR APD mean/sd	SVR APD mean/sd	MR Corr mean/sd	SVR Corr mean/sd
Chl <i>a</i>	52%/11%	38%/8%	0.36/0.2	0.53/0.2
MC	23%/8%	18%/5%	0.86/0.06	0.84/0.07
MUC	61%/18%	41%/11%	0.70/0.12	0.76/0.08
OM	47%/13%	35%/5%	0.77/0.07	0.72/0.1

Table 8 2005 ASD summary of regression results using five PCs

Property	MR APD mean/sd	SVR APD mean/sd	MR Corr mean/sd	SVR Corr mean/sd
Chl <i>a</i>	44%/10%	41%/8%	0.45/0.25	0.43/0.27
MC	38%/10%	33%/8%	0.59/0.14	0.57/0.16
MUC	52%/14%	48%/16%	0.67/0.11	0.66/0.12
OM	50%/13%	46%/9%	0.63/0.61	0.14/0.15

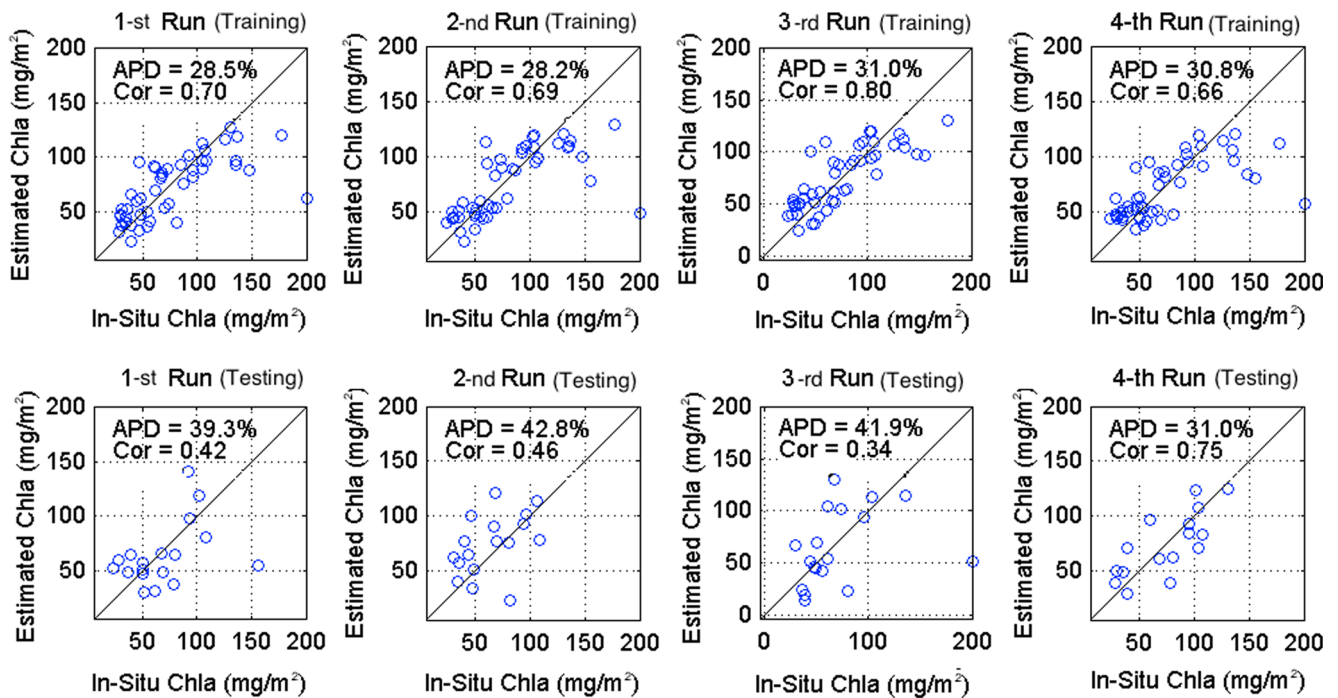


Fig. 4 Regression training and testing results for four runs of chl *a* SVR using all bands of 2005 ASD data

Table 9 2005 AHS Summary of regression results using all bands

Property	MR APD mean/sd	SVR APD mean/sd	MR Corr mean/sd	SVR Corr mean/sd
Chl <i>a</i>	117%/66%	47%/43%	0.06/0.44	0.37/0.51
MC	43%/27%	20%/6%	0.56/0.85	0.47/0.1
MUC	132%/116%	46%/20%	0.23/0.47	0.69/0.27
OM	223%/204%	40%/12%	0.26/0.49	0.77/0.11

Table 10 2005 AHS Summary of regression results using five PCs

Property	MR APD mean/sd	SVR APD mean/sd	MR Corr mean/sd	SVR Corr mean/sd
Chl <i>a</i>	59%/34%	54%/30%	0.29/0.31	0.22/0.3
MC	31%/16%	29%/14%	0.69/0.27	0.72/0.2
MUC	55%/27%	56%/27%	0.64/0.19	0.62/0.32
OM	66%/29%	49%/18%	0.64/0.26	0.72/0.16

Table 11 2013 ASD Summary of regression results using all bands

Property	MR APD mean/sd	SVR APD mean/sd	MR Corr mean/sd	SVR Corr mean/sd
Chl <i>a</i>	113%/62%	38%/14%	0.3/0.3	0.58/0.33
MC	58%/27%	22%/6%	0.45/0.3	0.62/0.25
MUC	273%/221%	49%/16%	0.22/0.34	0.6/0.26
OM	132%/72%	38%/18%	0.45/0.77	0.28/0.09

Table 12 2013 ASD Summary of regression results using five PCs

Property	MR APD mean/sd	SVR APD mean/sd	MR Corr mean/sd	SVR Corr mean/sd
Chl <i>a</i>	46%/11%	42%/8%	0.58/0.31	0.52/0.32
MC	24%/5%	20%/6%	0.46/0.22	0.51/0.23
MUC	55%/18%	48%/14%	0.49/0.15	0.51/0.24
OM	36%/9%	34%/7%	0.67/0.2	0.66/0.15

Table 13 2013 APEX summary of regression results using all bands

Property	MR APD mean/sd	SVR APD mean/sd	MR Corr mean/sd	SVR Corr mean/sd
Chl <i>a</i>	219%/223%	77%/29%	0.15/0.46	0.41/0.35
MC	51%/22%	33%/8%	0.25/0.42	0.27/0.43
MUC	77%/28%	45%/10%	0.52/0.34	0.61/0.2
OM	140%/297%	66%/49%	0.42/0.37	0.53/0.43

Table 14 2013 APEX summary of regression results using five PCs

Property	MR APD mean/sd	SVR APD mean/sd	MR Corr mean/sd	SVR Corr mean/sd
Chl <i>a</i>	95%/51%	82%/38%	0.37/0.35	0.3/0.31
MC	28%/11%	21%/6%	0.24/0.52	0.5/0.39
MUC	62%/20%	66%/23%	0.31/0.26	0.28/0.3
OM	75%/33%	83%/39%	0.36/0.38	0.3/0.4

corresponding imagery (e.g. Fig. 3). When PCA transformation was carried out for field spectra and imagery, the first five PCs were considered where their contribution to the variance in the data is shown in Table 6.

6.2 ASD, AHS, and APEX correlations to field data

Since several runs were done for each property, regressor, and considered dimensionality, the mean accuracy and standard deviation (sd) of the test results are reported in Tables 7 and 8 for ASD 2005 data. Figure 4 shows an example of the regression results (training and testing) for four runs of chl *a* content using 2005 ASD data.

Tables 9 and 10 show the results for 2005 AHS data. One can notice a great reduction in accuracy when compared to ASD data. Furthermore, when using all bands, SVR resulted in much better accuracy than MR. The use of PCA resulted in improvement in the MR results, yet did not impact SVR.

Tables 11 and 12 show the results for 2013 ASD data. MR using all spectral bands resulted in a very low accuracy that improved considerably when using five PCs. Tables 13 and 14 show the results for 2013 APEX data that show as well low accuracy when using all bands with MR.

It can be noticed that the best estimation is for moisture content since it results in relatively lower values of APD with a high Corr for all data. Furthermore, SVR showed a better capability of predicting the sediment properties than MR, and finally the use of PCA resulted in similar results when compared to using all the bands.

6.3 Mapping sediment properties using the airborne imagery

After testing the performance of the considered approaches, sediment property maps were created by estimating the values of each property using AHS and APEX imagery. All the data from the in-situ locations were used for the training of the regressor to create the maps.

Figures 5, 6, 7 and 8 show the resulting maps using the 2005 AHS image. Figures 9, 10, 11 and 12 show the resulting maps using the 2013 APEX image. For all properties, MR with all bands showed low performance. This can be due to overfitting the data. Further work needs to be done regarding this issue, yet it will not be carried out in the scope of this paper. Furthermore, for all maps and approaches (except for MR using all bands), special known features in the field such as those of saturated muddy areas or dry and sandy areas were revealed. Also from field knowledge, when PCs are used, it can be noticed that both regressors overestimated the values of all variables around the

Fig. 5 Chl *a* (mg/m²) maps for AHS 2005

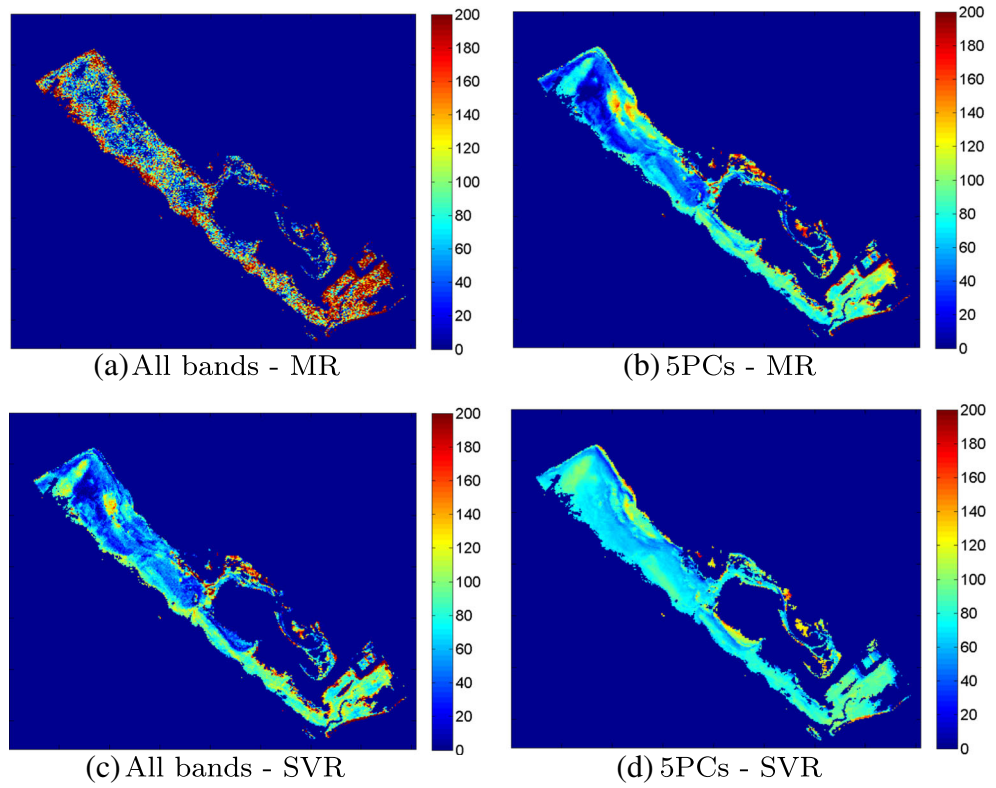


Fig. 6 Moisture content (%) maps for AHS 2005

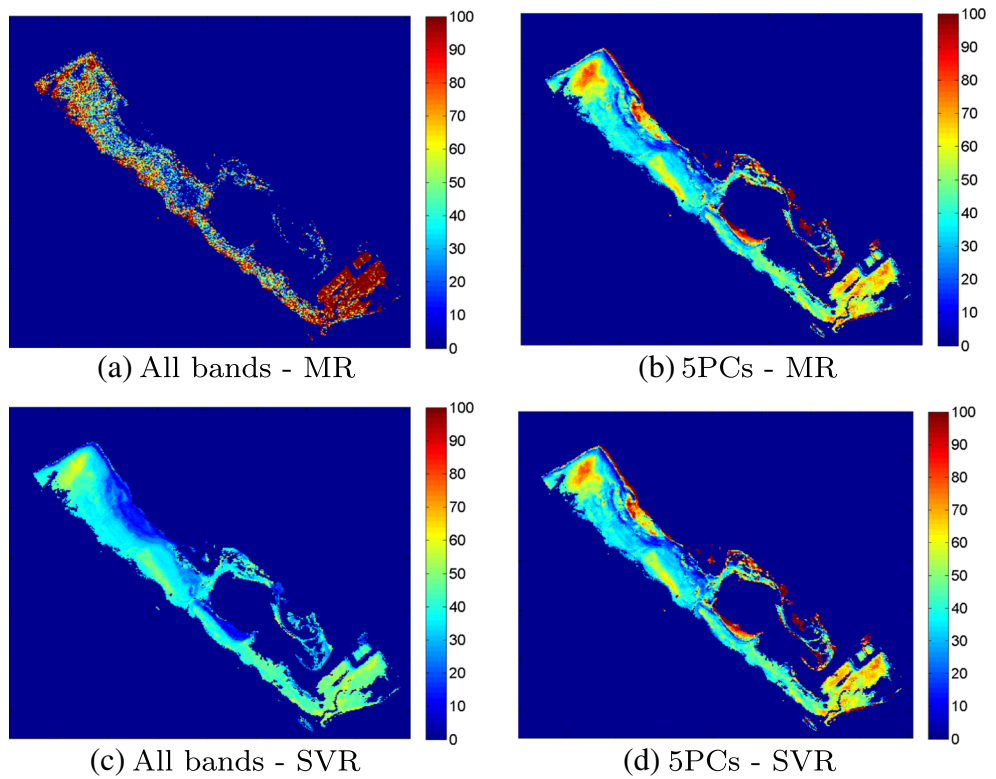


Fig. 7 Mud content (%) maps for AHS 2005

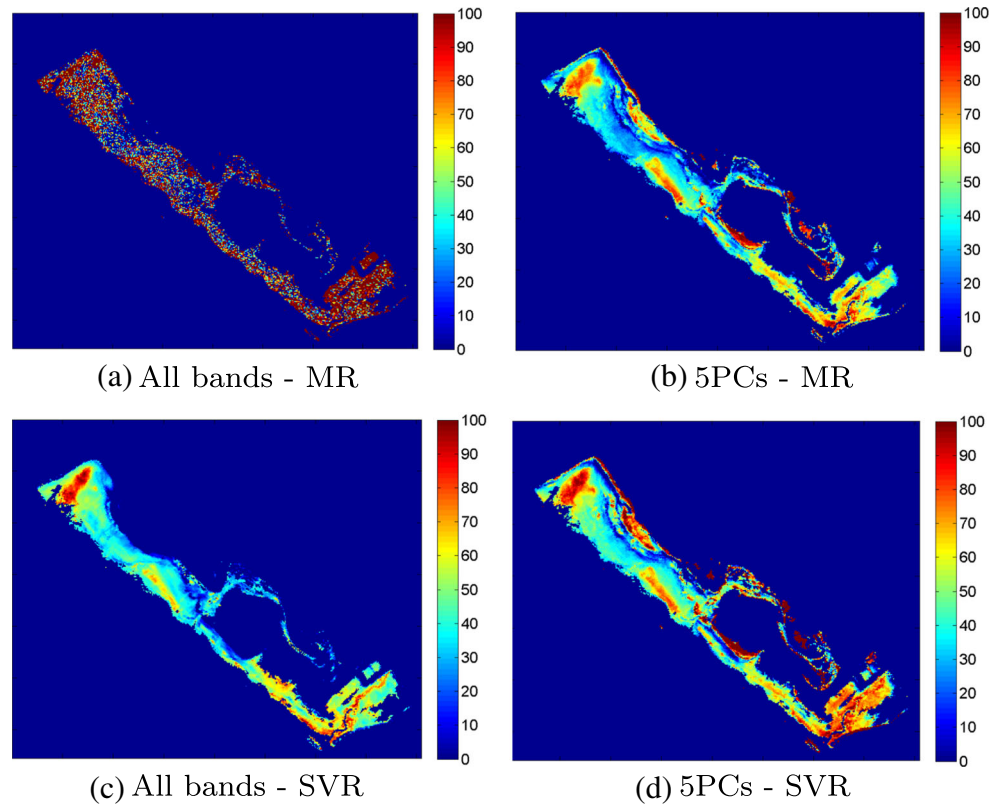


Fig. 8 Organic matter (%) maps for AHS 2005

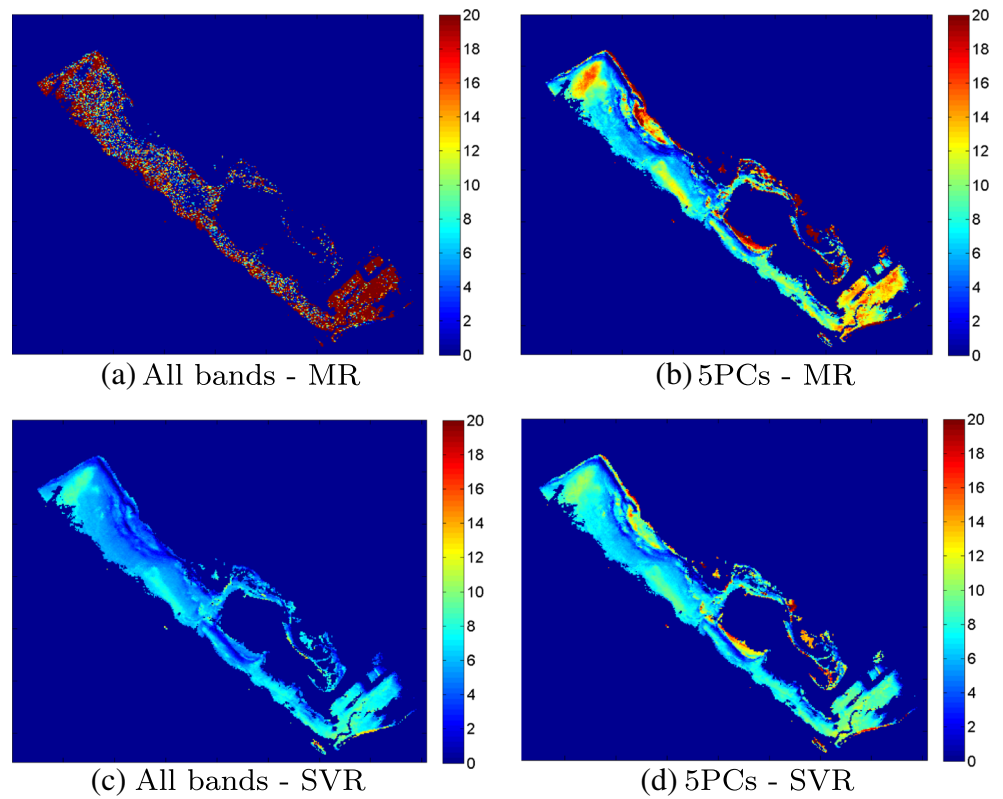


Fig. 9 Chl a (mg/m^2) maps for APEX 2013

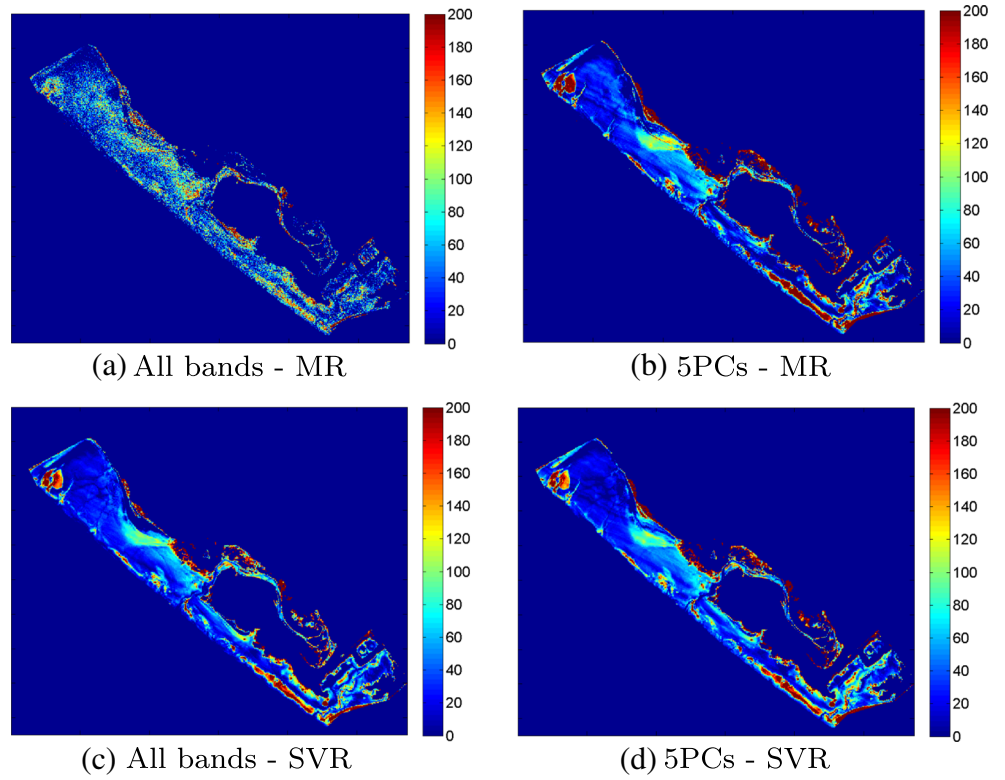


Fig. 10 Moisture content (%) maps for APEX 2013

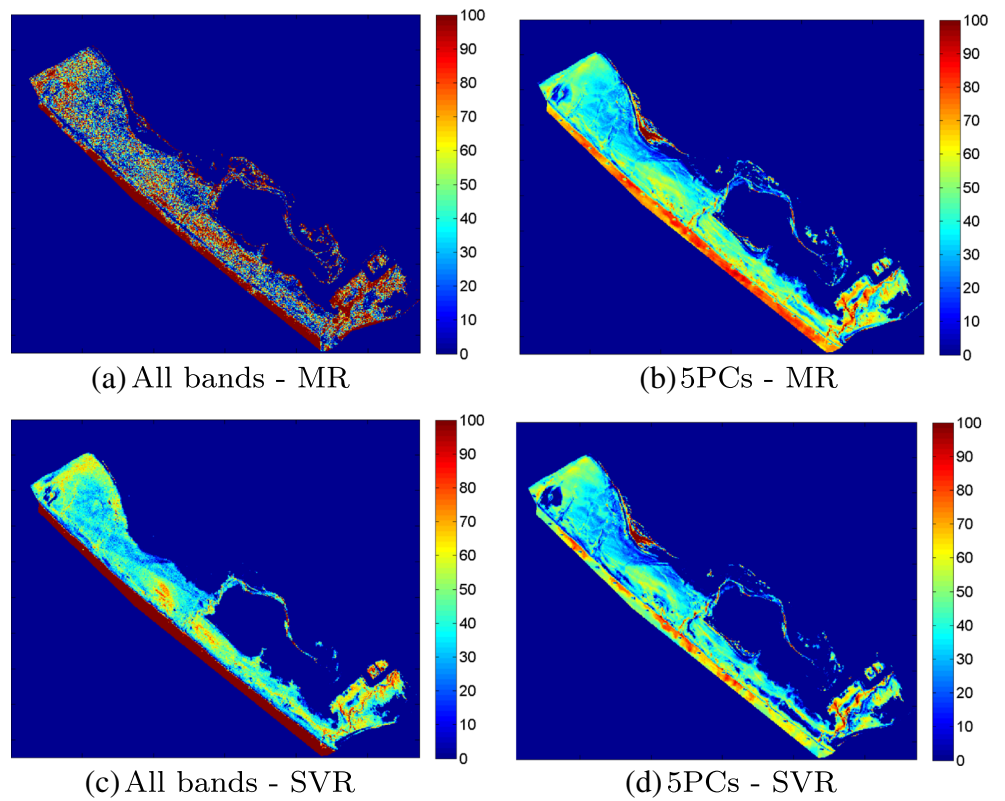


Fig. 11 Mud content (%) maps for APEX 2013

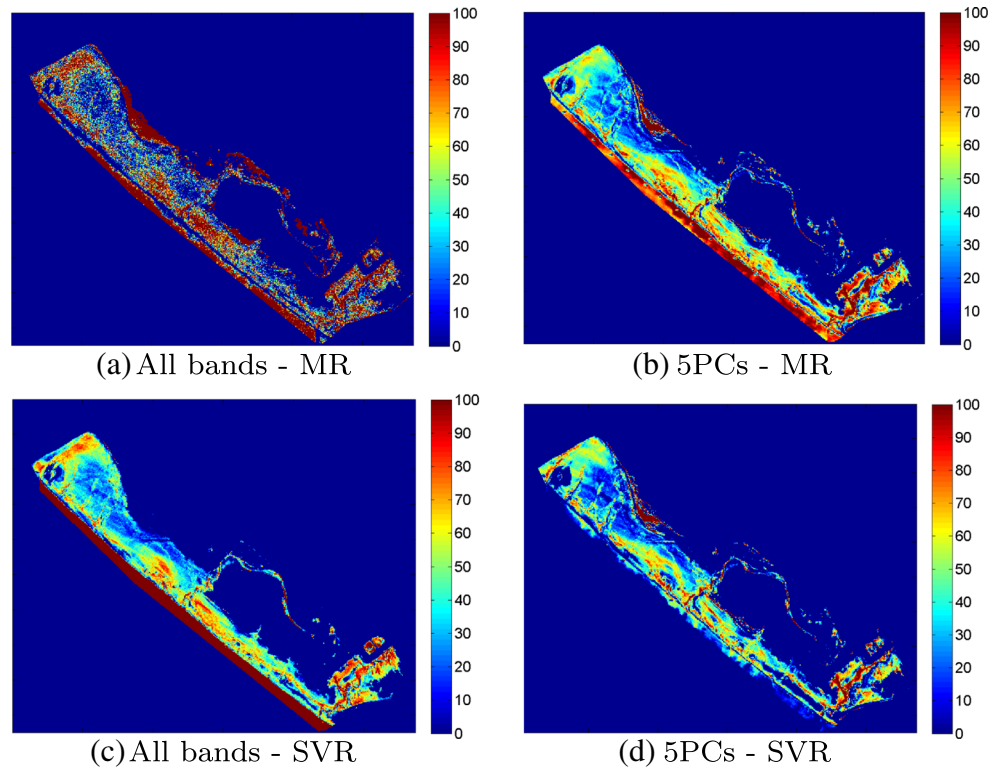
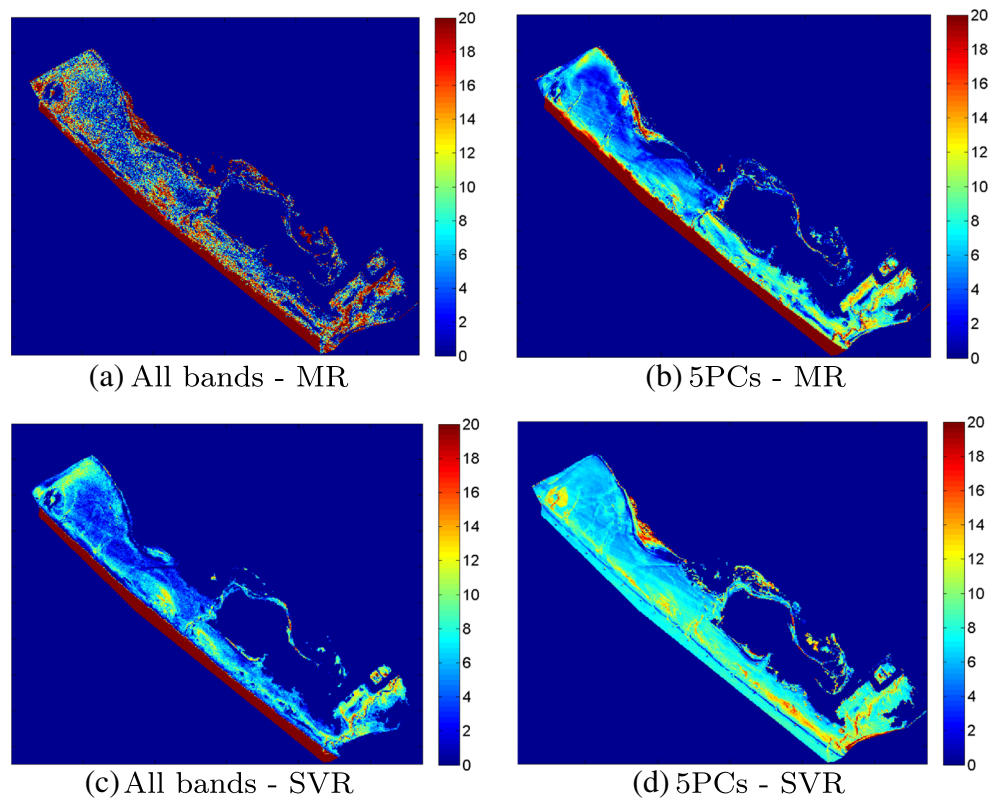


Fig. 12 Organic matter (%) maps for APEX 2013



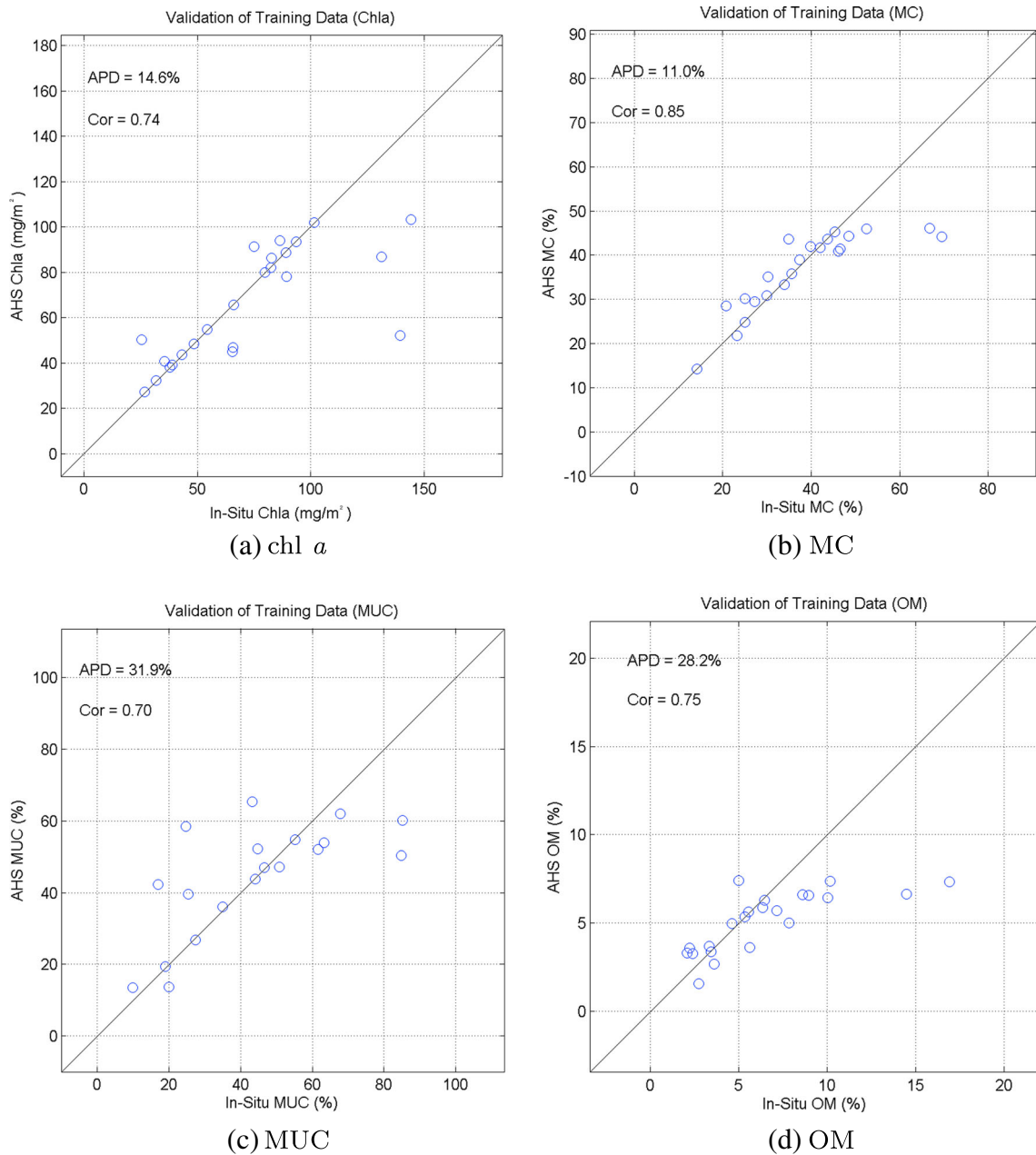


Fig. 13 Regression analysis using SVR and all bands of AHS 2005

North East borders of the flat. There, it can be that various bordering pixels may include vegetation or other dominating features that are accounted for in the regression. The regressors seem to give the highest values of each sediment property to those pixels. Yet, this overestimation is not revealed when SVR is used without PCA. Thus, SVR used with all bands seems to achieve the highest performance and the the best sediment maps. The regression plots of this approach as shown below in Figs. 13 and 14.

From the maps, it can be noticed that correlations between the different properties are revealed in several cases. For example, areas of very high mud content are typically accompanied with high moisture content. On the other hand, several areas of high chl *a* content close to the IJzer river consisted of low mud content. This is consistent with the field data and field spectra of MUC shown in Fig. 3 where chl *a* absorption features at about 673 nm (Murphy et al. 2005) is observed with relatively low mud content.

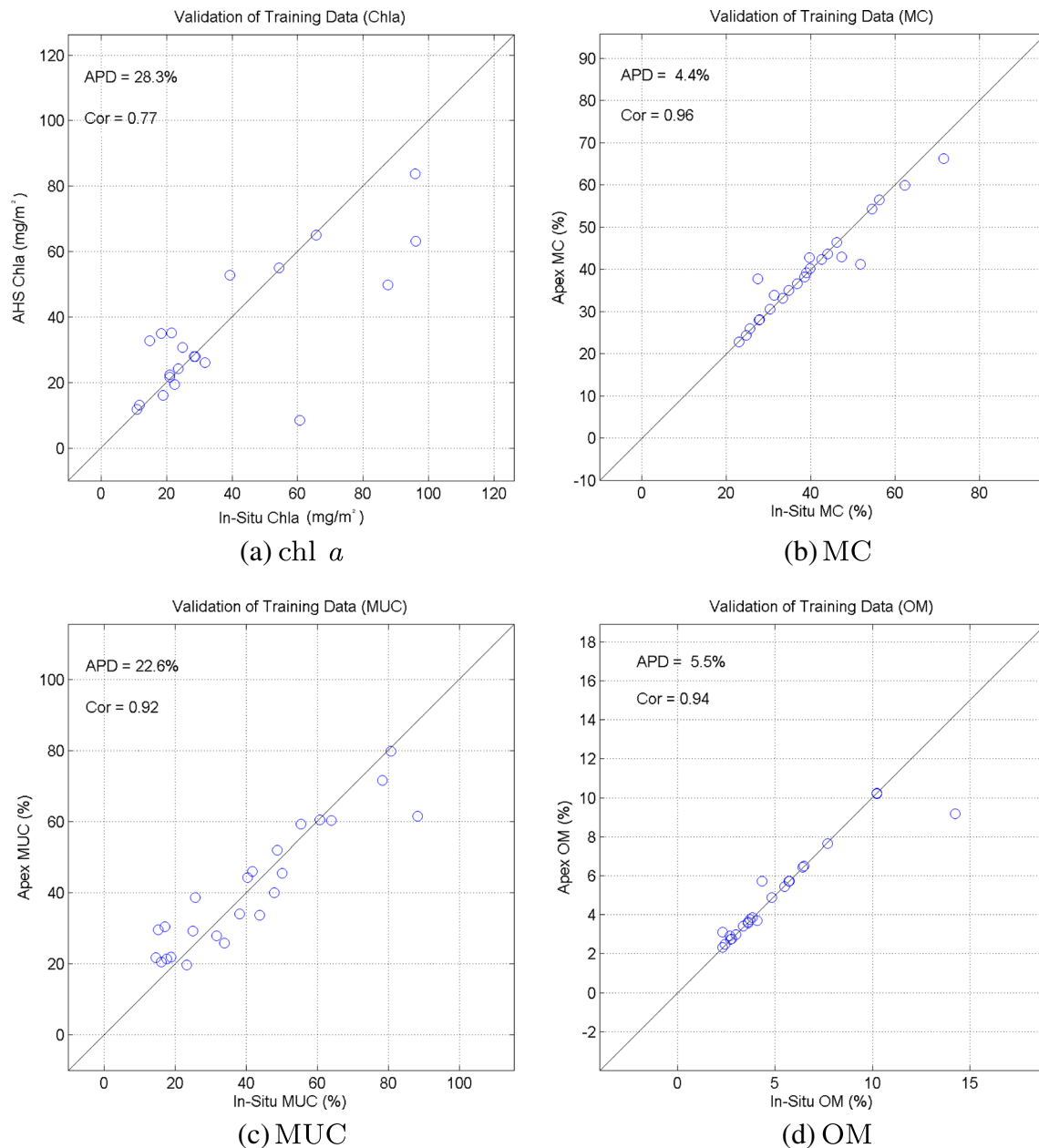


Fig. 14 Regression analysis using SVR and all bands of APEX 2013

6.4 Identifying important spectral features

Since MR resulted in reliable results only when feature reduction was considered, weights are calculated from this option. Figures 15 and 16 show weights retrieved for each band for that case. These weights or coefficients are obtained through a multiplication of the coefficients from PCA and MR as explained in the methodology, with $P = 5$.

The highest weights as an “absolute value” can be considered critical for estimating the corresponding variables.

Regarding the biological properties of sediments, an increase in chl *a* pigment leads to an emphasis around 440 nm and of the absorption dip at around 673 nm of the spectrum. This can be noticed in the obtained weights that the highest absolute values of weights are around those parts of the spectrum. Figure 17 shows examples of these spectra

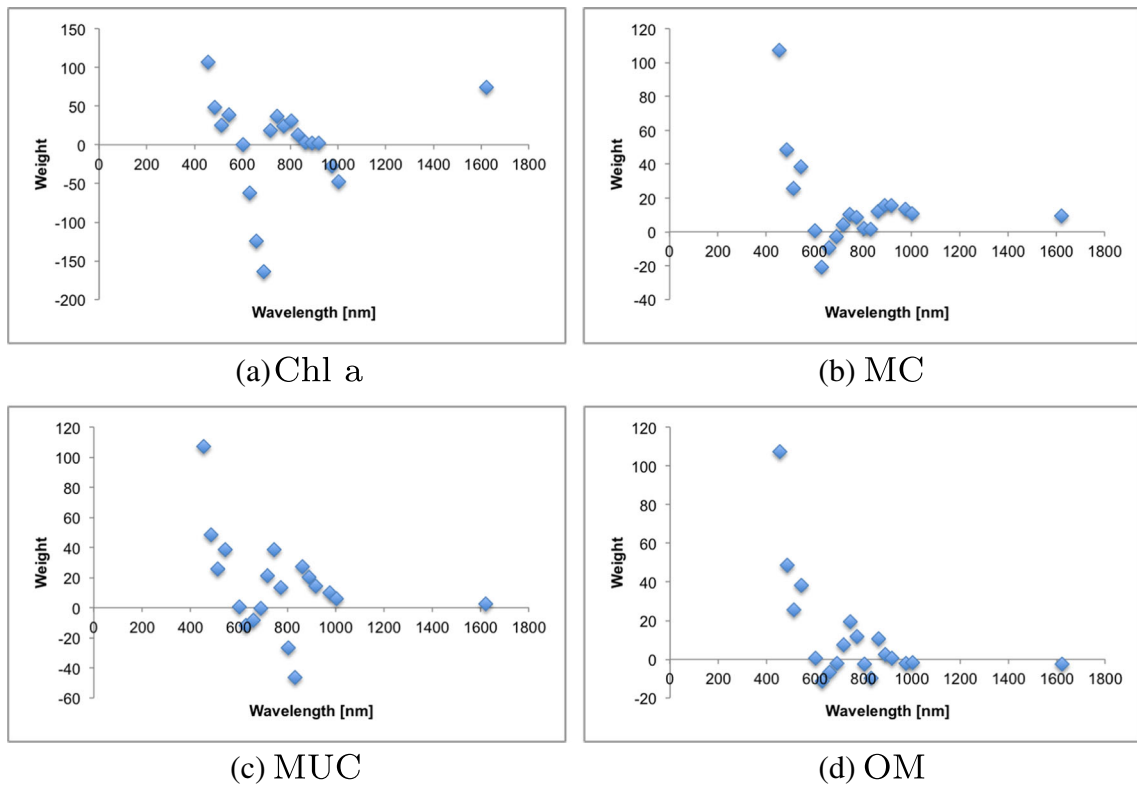


Fig. 15 Weights of different wavelengths of MR with five PCs of AHS 2005

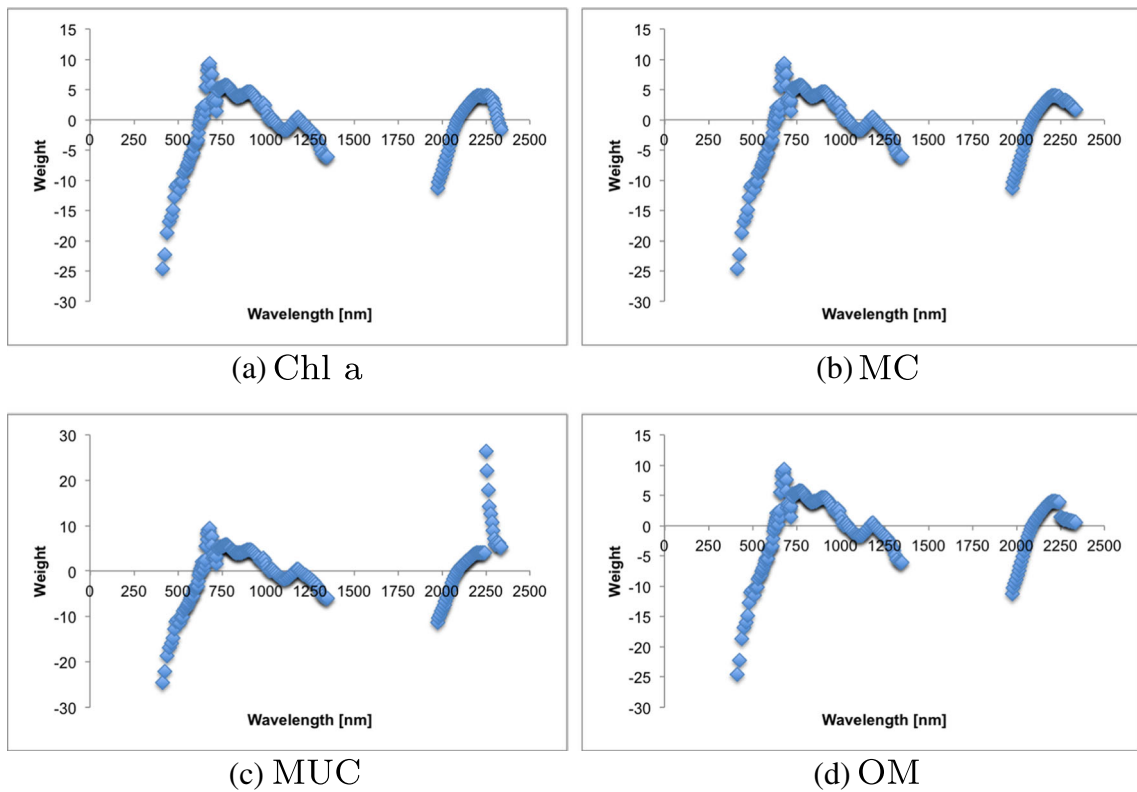


Fig. 16 Weights of different wavelengths of MR with five PCs of APEX 2013

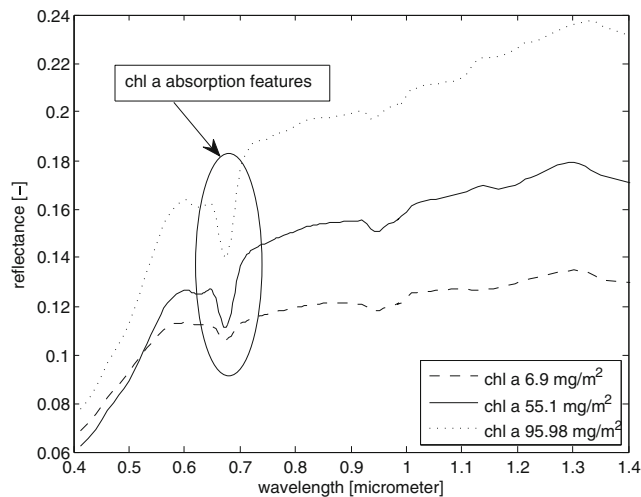


Fig. 17 2013 field spectra resampled to APEX bands for three samples showing low, average, and high values of chl *a* while other parameters (MC, MUC, and OM) were in the same range for the three

and the absorption features with varying content of chl *a* while moisture content is between 5 and 30% and MUC between 19 and 27%.

Furthermore, moisture content leads to an overall increase or decrease of the reflectance spectrum (Weidong et al. 2002; Neema et al. 1987). Yet, a special absorption feature is normally observed around 1450 nm (Adam et al. 2012). The spectral resolution of AHS does not allow the retrieval of this feature while the bands of APEX around that part of the spectrum have been excluded from the study for being too noisy. The resulting weights from the regression

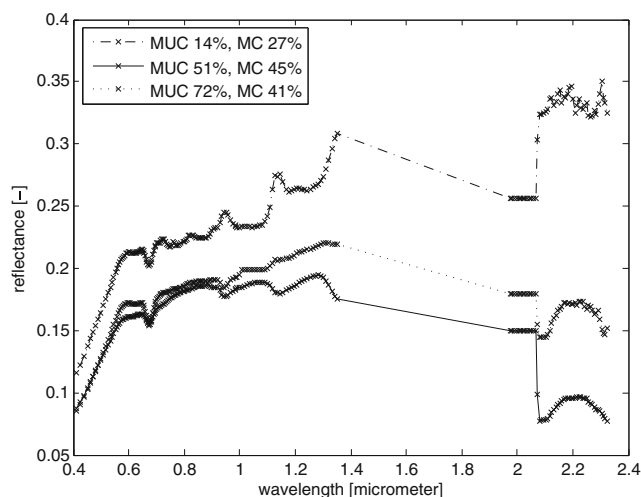


Fig. 18 2013 field spectra resampled to APEX bands for three samples showing low, average, and high values of MUC and their corresponding MC with chl *a* values varying between 20 and 30 mg/m²

show that the most important for moisture content of the available bands are of the shortest wavelengths.

The spectral response of increasing mud content in dry sediments consists of an increase in overall reflectance (Baumgardner et al. 1985) and an increase in absorption at specific clay absorption features (Hunt 1977). For a mix of fine sand with clay, absorption features have been reported between 1325 and 1563, 1850 and 2050, and 2125 and 2265 nm. AHS does not provide bands in those part so the spectrum. APEX bands include 2125 and 2265 nm and show great weight increase around these parts of the spectrum. Figure 18 shows spectral of varying values of MUC that can confirm this result when considering an absorption feature around 2125 nm yet an increase in reflectance around 2265 nm.

Regarding OM, generally, its effect is partially comparable to that of moisture content (Adam 2009). This can be retrieved from the weights of both images.

7 Conclusions

The regression approaches were successfully used to quantify four sediment properties, namely mud content, chlorophyll *a* concentration, organic matter content, and soil moisture for the IJzermonding. Multiple regression (MR) and support vector machine regression (SVR) with and without feature reduction were tested using in-situ and airborne hyperspectral signals. Then, sediment property maps of the IJzermonding nature reserve were created using airborne hyperspectral imagery. The results show the suitability of these approaches with the best results achieved when SVR was used with the full spectral dimensionality of the data. Furthermore, the work shows that PCA achieved in good results yet with an overestimation of sediment properties in pixels with unstudied features that are on the border of the intertidal flat. The importance of bands used for MR were also extracted as weights and showed comparable results to what is found in literature. This work is a foundation study for obtaining suitable approaches to model and assess changes in the intertidal flat using imagery of various sources from different periods. Such results would allow a better understanding of the temporal dynamics of the intertidal flat and result in valuable input for modelers and end-users.

Acknowledgments The field and flight campaigns were supported by the Belgian Science Policy Office in the framework of the STEREO programme, subsidy number SR/00/043, 109, and 072 and subsidy SR/67/167 (BELAIR2013) / SR/XX/169 (BELAIR LITORA).

References

- Adam S (2009) Bio-physical characterization of sediment stability indicators for mudflats using remote sensing. Ph.D. thesis, Katholieke Universiteit Leuven, Belgium
- Adam S, Monbaliu J, Toorman E (2012) Quantification of bio-physico-chemical properties of intertidal sediment at different spatial scales using remote sensing. *International Journal of Remote Sensing* (2012):37–41
- Adam S, Vitse I, Johannsen C, Monbaliu J (2006) Sediment type unsupervised classification of the Molenplaat, Westerschelde estuary, the Netherlands. *EARSeL eProceed* 5:146–160
- Amos C, Feeney T, Sutherland T, Luternauer J (1997) The stability of fine-grained sediments from the Fraser River Delta. *Estuar, Coast Shelf Sci* 45:507–524
- Barille L, Mouget JLL, Meleder V, Rosa P, Jesus B, Barillé L., Méléder V. (2011) Spectral response of benthic diatoms with different sediment backgrounds. *Remote Sens Environ* 115:1034–1042. doi:10.1016/j.rse.2010.12.008
- Baumgardner M, Silva L, Biehl L, Stoner E (1985) Reflectance properties of soils. *Adv Agron* 38:1–44
- Defew E, Tolhurst T, Paterson D (2002) Site-specific features influence sediment stability of intertidal flats. *Hydrol Earth Syst Sci* 6:971–982
- Deronde B, Kempeneers P, Forster R (2006) Imaging spectroscopy as a tool to study sediment characteristics on a tidal sandbank in the Westerschelde. *Estuar, Coast Shelf Sci* 69:580–590
- Diafas I, Panagos P, Montanarella L (2013) Willingness to pay for soil information derived by digital maps: A choice experiment approach. *Vadose Zone Journal*:1–8
- Draper N, Smith H (1998) *Applied regression analysis*, 3rd edn. Wiley
- Drucker H, Burges C, Kaufman L, Smola A, Vapnik N (1996) *Support vector regression machines*. *Advances in Neural Information Processing Systems*, MIT press, Cambridge
- Flemming BW (2000) A revised textural classification of gravel-free muddy sediments on the basis of ternary diagrams. *Cont Shelf Res* 20:1125–1137
- Gege P, Fries J, Haschberger P, Schotz P, Schwarzer H, Strobl P, Suhr B, Ulbrich G, Vreeling WJ (2009) Calibration facility for airborne imaging spectrometers. [ISPRS] *J Photogramm Remote Sens* 64:387 – 397. doi:10.1016/j.isprsjprs.2009.01.006. <http://www.sciencedirect.com/science/article/pii/S0924271609000124>
- Giardino A, Ibrahim E, Adam S, Toorman E, Monbaliu J (2009) Hydrodynamics and cohesive sediment transport in the ijzer estuary. *Belgium J Waterway, Port Coast, Ocean Eng* 135(4):176–184
- Hakvoort H, Heymann K, Stein C, Murphy D (1997) In-situ optical measurements of sediment type and phytobenthos of tidal flats: a basis for imaging remote sensing spectroscopy. *Deut Hydrographische Z / German J Hydrogr* 49:367–373
- Hakvoort JHM, Heineke M, Heymann K, Kuhl H, Riethmüller R., Witte G (1998) Optical remote sensing of microphytobenthic biomass: a method to monitor tidal flat erodibility. *Senckenberg Marit* 29:77–85
- Herman P, Middelburg J, Heip C (2001) Benthic community structure and sediment processes on an intertidal flat: results from the ecoflat project. *Cont Shelf Res* 21:2055–2071
- Herrier J. L., Nieuwenhuys HV (2005) The Flemish coast : life is beautiful ! *Nature* 200(2000):13–26
- Hoffman M, Adam S, Baert L, Bonte D, Chavatte N, Claus R, De Belder W, De Fre B, Degraer S, De Groot D, Dekoninck W, Desender K, Devos K, Engledow H, Grootaert P, Hardies N, Leli-aert F, Maelfait JP, Monbaliu J, Pollet M, Provoost S, Stichelmanns E, Toorman E, Van Nieuwenhuys H, Vercruysse E, Vinckx M, Wittoeck J (2005) Integrated monitoring of nature restoration along ecotones, the example of the Yser estuary. In: *Proceedings 'Dunes and Estuaries 2005' - International conference on Nature Restoration Practices in European Coastal Habitats*, Koksijde, Belgium, pp. 191–208
- Hunt G (1977) Spectral signatures of particulate minerals in the visible and near infrared. *Geophysics* 42:501–513
- Ibrahim E, Adam S, De Wever A, Govaerts A, Vervoort A, Monbaliu J (2014) Investigating spatial resolutions of imagery for intertidal sediment characterization using geostatistics. *Cont Shelf Res* 85:117–125
- Ibrahim E, Monbaliu J (2009) Supervised classification of hyperspectral images of algased. Report, Vlaams Instituut voor de Zee (VLIZ). prefixwww.vliz.be/imisdocs/publications/238876.pdf
- Ibrahim E, Monbaliu J (2013) Site-dependent classes for the classification of intertidal sediments. In: *33rd EARSeL Symposium, Towards Horizon 2020*, Matera, Italy, p 773:782
- Jolliffe I (1986) *Principal component analysis*. Springer, New York
- Kumar S, Ghosh J, Crawford M (2001) Best-bases feature extraction algorithms for classification of hyperspectral data. *IEEE Trans Geosci Remote Sens* 39:1368–1379
- Lillesand T, Kiefer R (2015) *Remote sensing and image interpretation*, 7th edn. Wiley
- Lundkvist M, Grue M, Friend P, Flindt M (2007) The relative contributions of physical and microbiological factors to cohesive sediment stability. *Cont Shelf Res* 27:1143–1152
- Mitchener H, Torfs H (1996) *Erosion of mud/sand mixtures*, vol 29, pp 1–25
- Murphy R, Tolhurst T, Chapman M, Underwood A (2009) Seasonal distribution of chlorophyll on mudflats in new south wales, Australia measured by field spectrometry and pam fluorometry. *Estuar Coast Shelf Sci* 84:108–118
- Murphy R, Tolhurst T, Chapman M, Underwood A (2005) Estimation of surface chlorophyll a on an emersed mudflat using field spectrometry: accuracy of ratios and derivative-based approaches. *Int J Remote Sens* 26:1835–1859
- Neema D, Shah A, Patel A (1987) A statistical model for light reflection and penetration through sand. *Int J Remote Sens* 8:1209–1217
- Rainey M, Tyler A, Gilvear D, Bryant R, McDonald P (2003) Mapping intertidal estuarine sediment grain size distributions through airborne remote sensing. *Remote Sens Environ* 86:480–490
- Richter R, Schläpfer D. (2002) Geo-atmospheric processing of airborne imaging spectrometry data. Part 2, Atmospheric/topographic correction. *Int J Remote Sens* 23:2631–2649
- Smith GM, Thomson A, Möller I., Kromkamp JC (2004) Using hyperspectral imaging for the assessment of mudflat surface stability. *J Coast Res* 20:1165–1175
- Thomson A, Fuller R, Yates M, Brown S, Cox R, Wadsworth R (2003) The use of airborne remote sensing for extensive mapping of intertidal sediments and saltmarshes in eastern England. *Int J Remote Sens* 24:2717–2737
- Van der Wal D, Herman P (2007) Regression-based synergy of optical, shortwave, infrared and microwave remote sensing for monitoring the grain-size of intertidal sediments. *Remote Sens Environ* 111:89–106

- Weidong L, Baret F, Xingfa G, Qingxi T, Lanfen Z, Bing Z (2002) Relating soil surface moisture to reflectance. *Remote Sens Environ* 81:238–246
- Widdows J, Brinsley M (2002) Impact of biotic and abiotic processes on sediment dynamics and the consequences to the structure and functioning of the intertidal zone. *J Sea Res* 48:143–156
- Wright S, Jeffrey S, Mantoura R, Llewellyn C, Bjornland T, Repeat D, Welshmeyer N (1991) Improved HPLC method for the analysis of chlorophylls and carotenoids from marine phytoplankton. *Mar Ecol Progress Ser* 77:183–196
- Yates M, Jones A, McGrorty S, Goss-Custard J (1993) The use of satellite imagery to determine the distribution of intertidal surface sediments of the Wash, England. *Estuar, Coast Shelf Sci* 36:333–344